JOC The Journal of Organic Chemistry

pubs.acs.org/joc Article

Mechanistic Insights into Formation of All-Carbon Quaternary Centers via Scandium-Catalyzed C−H Alkylation of Imidazoles with 1,1-Disubstituted Alkenes

Jiandong Guo, Wu Yang, Dongju Zhang, Shou-Guo Wang, and Xiaotai Wang*

Cite This: https://dx.doi.org/10.1021/acs.joc.0c03054 Read Online

ACCESS | Metrics & More | Article Recommendations | Supporting Information

ABSTRACT: This density functional theory (DFT) study reveals a detailed plausible mechanism for the Sc-catalyzed C−H cycloaddition of imidazoles to 1,1-disubstituted alkenes to form all-carbon quaternary stereocenters. The Sc complex binds the imidazole substrate to enable deprotonative C2−H bond activation by the Sc-bound α-carbon to afford the active species. This complex undergoes intramolecular cyclization (C═C into Sc−imidazolyl insertion) with exo-selectivity, generating a β-all-carbon-substituted quaternary center in the polycyclic imidazole derivative. The Sc-bound α-carbon deprotonates the imidazole C2−H bond to deliver the product and regenerate the active catalyst, which is the rate-determining step. Calculations illuminate the electronic effect of the ancillary Cp ligand on the catalyst activity and reveal the steric bias caused by using a chiral catalyst that induce the enantioselectivity. The insights can have implications for advancing rare-earth metal-catalyzed C−H functionalization of imidazoles.

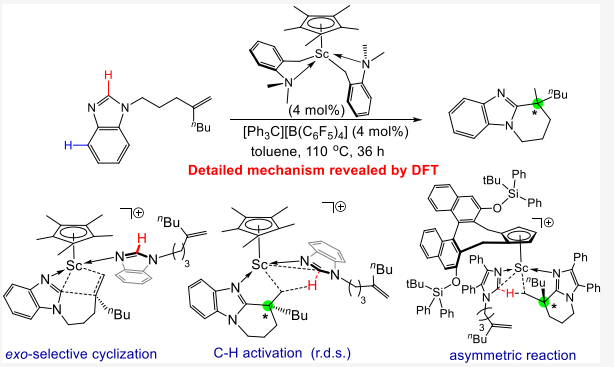

1. INTRODUCTION

All-carbon quaternary centers are a key structural element of many bioactive compounds and natural products, and the efficient and selective construction of such carbon-substituted stereocenters has attracted intense interest.[1,2] Imidazoles are an important class of heterocycles with biological significance and applications,[3] and as such, imidazole derivatives bearing all-carbon quaternary centers are valuable synthetic targets. In theory, the C2−H bond of an imidazole could be utilized for a Markovnikov addition to a 1,1-disubstituted alkene to form, in a fully atom-economic manner, a derivative with an all-carbon quaternary stereocenter; however, such an approach had not been realized until Hou and co-workers reported in 2020 the scandium-catalyzed formal intramolecular C−H alkylation of imidazoles with 1,1-disubstituted alkenes (Scheme 1).[4,5] This excellent work, which is built upon the Hou group's earlier success in utilizing half-sandwich rare-earth complexes for catalyzing C−H addition to alkenes,[6,7] represents a significant advance in the areas of quaternary carbon center construction and C−H functionalization of imidazoles by rare-earth metal catalysis.

Hou et al. proposed a mechanistic outline for the reaction, which involves key steps such as the deprotonative C−H activation by the Sc-bound alkyl (an internal base) and the intramolecular insertion (i.e., cyclization) of the C═C unit into the Sc−imidazolyl bond. Their deuterium-labeling experiments suggested involvement of C−H bond cleavage in the rate-determining step.[4] There are intriguing mechanistic questions about this catalytic reaction that deserve in-depth investigations. For example, the unsubstituted cyclopentadienyl (Cp) ligand reduces the catalyst activity significantly (Scheme 1a). How is this ligand effect accounted for? In addition, the C−H activation is chemoselective and occurs at the C2 carbon position, and the subsequent cyclization is regioselective (i.e., exo-selective). Finally, the chiral catalyst **CAT3** achieves asymmetric cyclization, affording the bicyclic imidazole derivative bearing a chiral all-carbon quaternary stereocenter with high enantioselectivity (Scheme 1b). What are the origins of the chemo-, regio-, and enantioselectivities? In this theoretical study, we address the above questions via density functional theory (DFT) calculations on the representative reactions shown in Scheme 1. We aim to establish a detailed plausible mechanism that elucidates the workings of the title reaction and provides valuable insights into Sc-catalyzed C−H functionalization of imidazole compounds.

Received: December 29, 2020

Scheme 1. Sc-Catalyzed Imidazole C−H to C=C Cycloaddition Leading to Formation of All-Carbon Quaternary Centers

a. General reaction conditions

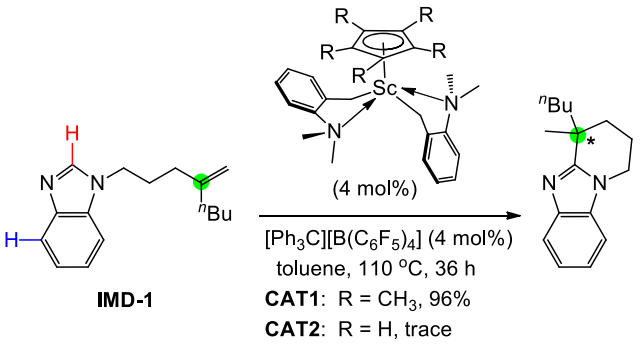

b. Asymmetric transformation

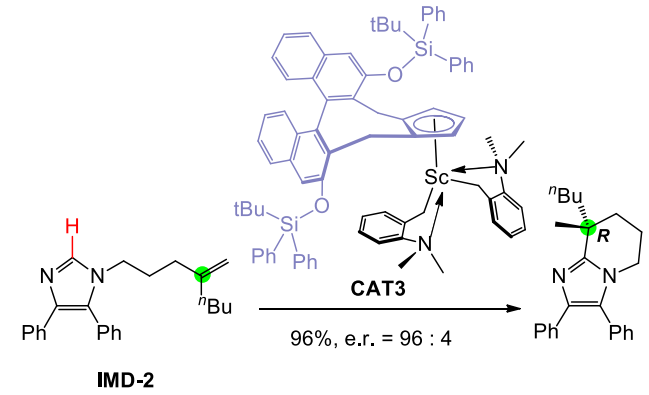

2. COMPUTATIONAL METHODS

All calculations were performed with Gaussian 09.[8] The functional M06-L,[9] suitable for applications in transition metal chemistry,[10] has been successfully used in numerous studies on transition metal-catalyzed organic reactions.[11−21] It was combined with the dispersion correction D3[22] in this work to enhance computational accuracy. Structures were optimized and characterized by frequency calculations to be energy minima (zero imaginary frequencies) or transition states (only one imaginary frequency) at the M06-L-D3/6-31G(d,p) level with the solvent (toluene) effects included using the SMD[23] solvation model. Quasi-harmonic approximations were made for the low-energy vibrational modes of the large molecules (≥ 172 atoms) involved in the asymmetric reaction using Truhlar corrections[24] for all frequencies below 100 cm^{-1} performed with the Shermo software package.[25] The energies were refined by M06-L-D3/6-311++G(d,p)/SMD(toluene) single-point calculations. The refined energies were converted to zero-point energy-corrected free energies at 110 °C (383.15 K) and 1 atm. Benchmark DLPNO-CCSD(T)[26] calculations were performed on the key intermediates and transition states of the **CAT1**- and **CAT2**-catalyzed reactions, and the results were consistent with those obtained with M06-L-D3 (Figure S1). Selected molecular structures were illustrated with CYLview.[27] Electrostatic potentials and electron density contour plots were obtained with Multiwfn.[28]

3. RESULTS AND DISCUSSION

3.1. Precatalyst Initiation. The additive $[Ph_3C][B(C_6F_5)_4]$ plays a vital role in activating the precatalyst **CAT1**. As shown in Figure 1, the Ph_3C^+ cation attacks one of the Sc-bound α-carbon atoms via the transition state **TS1** that contains a partially broken Sc−C bond at 2.87 Å and an incipient C−C bond at 2.57 Å. **TS1** proceeds to the cationic complex **IM1** with the extrusion of the arylamine byproduct. The enhanced coordinating power of cationic **IM1** is manifested by its highly exergonic uptake of the imidazole substrate **IMD-1** to form two possible isomeric complexes, **IM2a** and **IM2b**.

We envisioned that **IM2a** and **IM2b** could correspondingly introduce the C2−H (red) and C3−H (blue) activation via a transition state in which the remaining Sc-bound α-carbon acts as an internal base to cleave the C−H bond. We then estimated the acidity of the C2−H and C3−H bonds of **IMD-1** by calculating the electrostatic potentials of the hydrogen atoms.[29] The results of −29.35 eV for the C2-attached hydrogen and

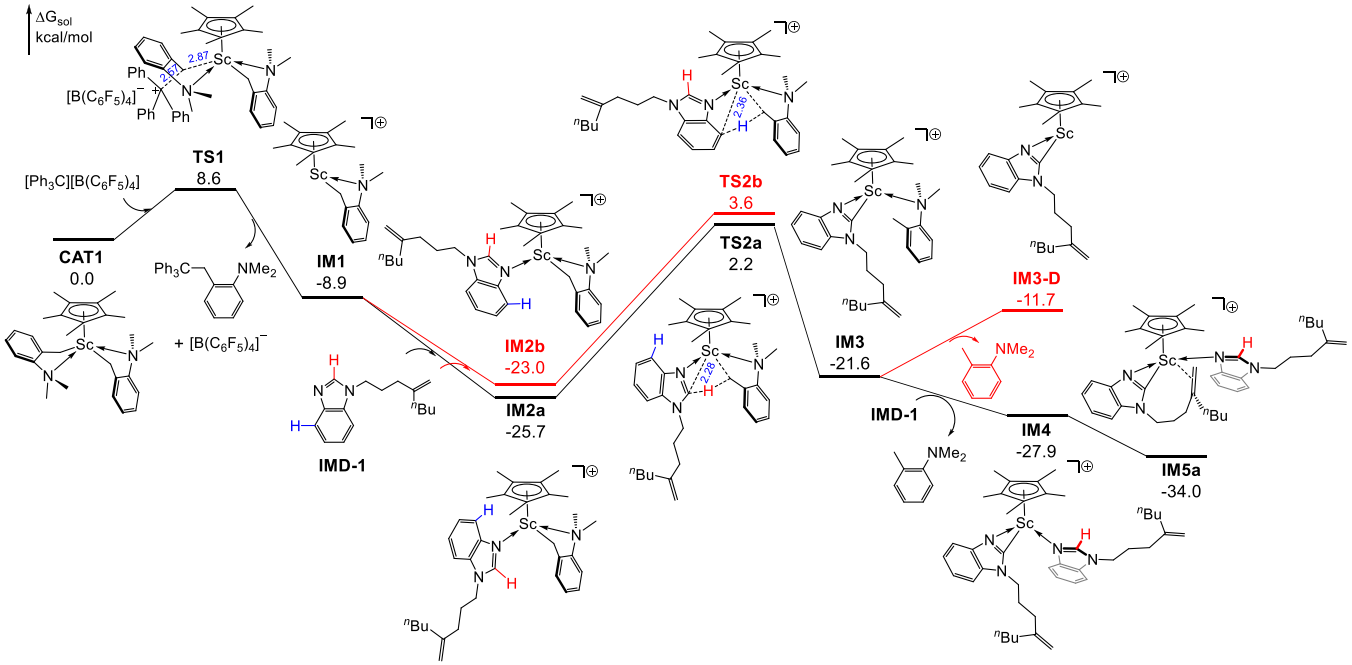

Figure 1. Free energy profile for the initiation process of **CAT1**. Selected bond distances in blue font are given in Å (the same below).

https://dx.doi.org/10.1021/acs.joc.0c03054
J. Org. Chem. XXXX, XXX, XXX−XXX

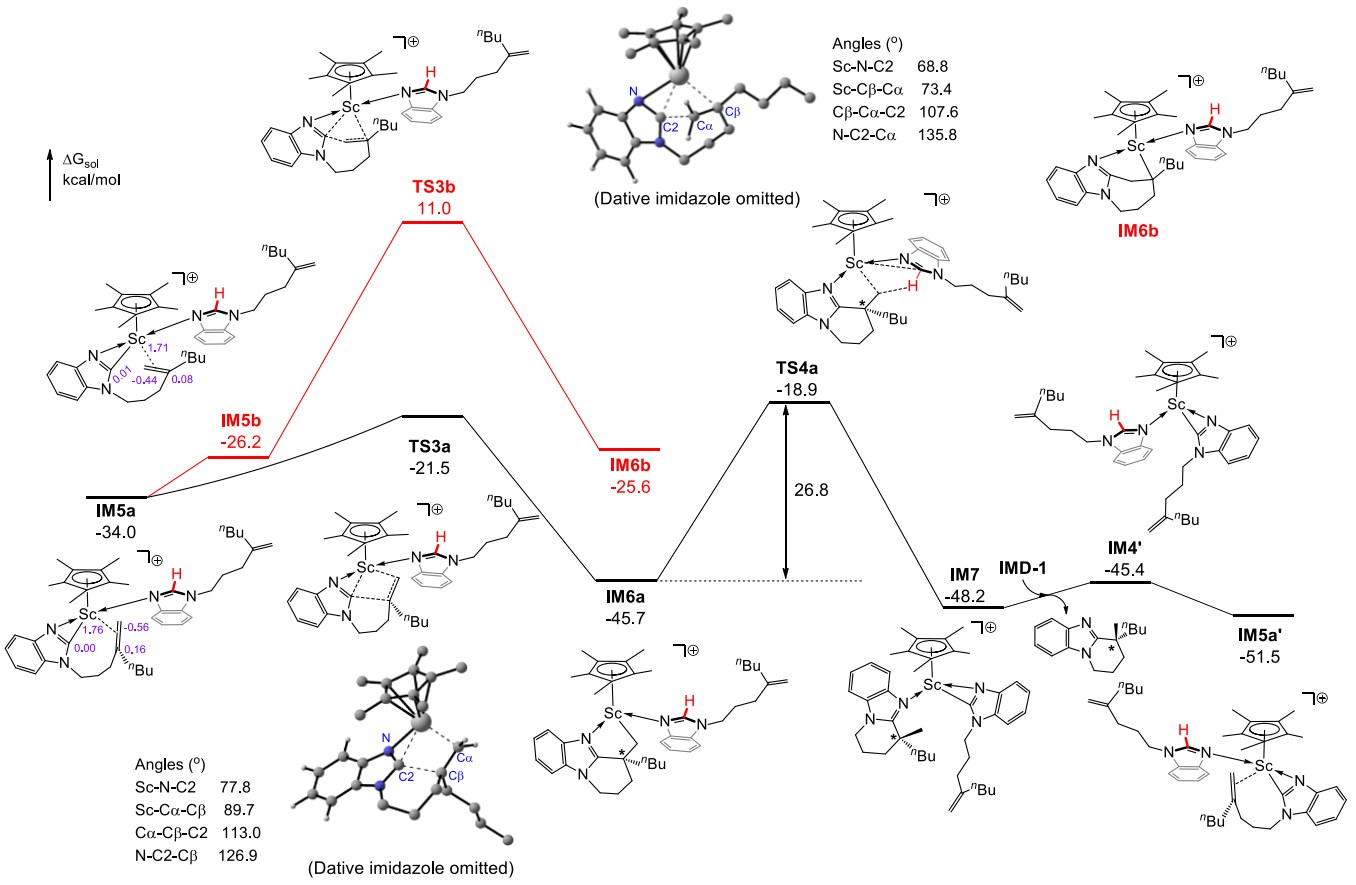

Figure 2. Free energy profile for the catalytic pathway consisting of cyclization, C−H activation, and catalyst regeneration. The numbers shown in purple font denote natural charges on selected atoms in **IM5a** and **IM5b**. **IM4′** and **IM5a′** are mirror inverts of **IM4** and **IM5a** (see Figure 1), respectively.

−30.61 eV for the C3-attached hydrogen indicate that the C2−H bond is more acidic and deprotonatable than the C3−H bond. This prediction agrees with the relative energies of the transition states **TS2a** for C2−H activation and **TS2b** for C3−H activation (**TS2a** is lower than **TS2b** by 1.4 kcal/mol). Therefore, the calculations qualitatively explain the experimentally observed chemoselectivity. **TS2a** and **TS2b** can be viewed as five-membered and six-membered chelate ring structures, respectively, with the former being energetically more favorable than the latter. The emerging Sc−C2 bond at 2.28 Å in **TS2a** is shorter and stronger than the Sc−C3 bond at 2.36 Å in **TS2b**. Such are the structural origins of the selective C2−H activation. **TS2a** proceeds to the imidazolyl complex **IM3** bearing an arylamine ligand (o-$MeC_6H_4NMe_2$). Dissociation of o-$MeC_6H_4NMe_2$ from **IM3** to form **IM3-D** would be endergonic by 9.9 kcal/mol, suggesting that the Sc^{III} d^0 center in **IM3** and its derivatives favors relatively high coordination numbers. Substitution of **IMD-1** for o-$MeC_6H_4NMe_2$ converts **IM3** into the more stable complex **IM4** (ΔG = −6.3 kcal/mol).[30] **IM4** undergoes intramolecular C═C to Sc π-coordination, forming **IM5a** and bringing the C═C unit into contact with the Sc−imidazolyl bond.[31] **IM5a** is the most stable species, the catalyst resting state, generated in the highly exergonic initiation process (ΔG = −34.0 kcal/mol). The largest energy span[32] along the computed initiation profile is from **IM2a** to **TS2a**, 27.9 kcal/mol, which is consistent with the reaction temperature (110 °C).

3.2. Catalytic Pathway. As shown in Figure 2, **IM5a** and its isomer **IM5b** could undergo intramolecular insertions (cyclizations) of the C═C unit into the Sc−imidazolyl bond via **TS3a** and **TS3b**, respectively. The exo-selective **TS3a** is lower in energy than the endo-selective **TS3b** by 32.5 kcal/mol, so there is an overwhelming preference for exo-cyclization, leading to the formation of **IM6a** with a six-membered ring bearing an all-carbon quaternary stereocenter as marked. The regioselectivity originates in part from the electrostatic dipole−dipole interaction between the Sc−C and C═C bonds that favors the exo-selective cyclization. We have analyzed the natural charges on the atoms of the Sc−C and C═C bonds in precursors **IM5a** and **IM5b** (Figure 2). The Sc−C bond in **IM5a**/**IM5b** has a positive charge on Sc (1.76/1.71) and essentially zero charges on C. The C═C bond has a partial positive charge on the internal carbon (0.16/0.08) and a partial negative charge on the terminal carbon (−0.56/−0.44); that is, the C═C bond is polarized by the electron-donating n-butyl substituent on the internal carbon. These natural charge distributions suggest that the $Sc^{1.76+}$−$C^{0.56-}$ (terminal) attractive interaction in **IM5a** with the exo-selective orientation is tremendously favored over the $Sc^{1.71+}$−$C^{0.08+}$(internal) repulsive interaction in **IM5b** with the endo-selective orientation. Therefore, the electronic factors very much favor the exo-selective cyclization via **TS3a**. We have also identified another important contributing factor to the energetic difference between **TS3a** and **TS3b**; that is, the emerging five-membered chelate ring of **TS3b** contains greater ring strain than that of **TS3a**, as illustrated by the ball-and-stick representations and the selected bond angles (Figure 2). Specifically, the N-C2-Cα angle

https://dx.doi.org/10.1021/acs.joc.0c03054
J. Org. Chem. XXXX, XXX, XXX−XXX

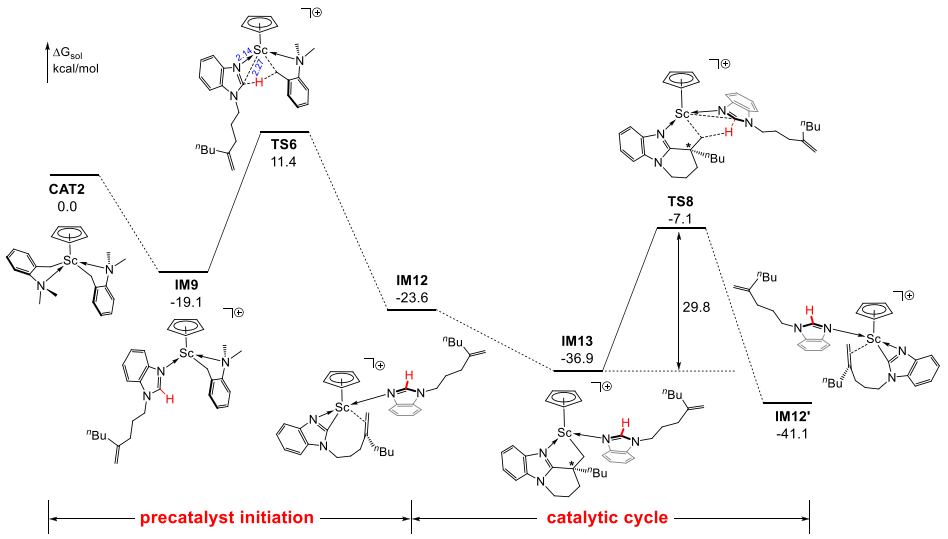

Figure 3. Free energy profile for a shortened **CAT2**-catalyzed pathway showing the key energetics (see Figure S2 for the complete reaction pathway).

of **TS3b** (135.8°) deviates more from 120° as compared with the corresponding N-C2-Cβ angle of **TS3a** (126.9°), and the Sc-N-C2, Sc-Cβ-Cα, and Cβ-Cα-C2 angles of **TS3b** are each smaller and more strained than the analogous Sc-N-C2, Sc-Cα-Cβ, and Cα-Cβ-C2 angles of **TS3a**. The cyclization intermediate **IM6a** leads into **TS4a** in which the Sc-bound α-carbon acts as an internal base to cleave the C2−H bond of the bound imidazole **IMD-1**. **TS4a** proceeds to **IM7** that bears the imidazolyl anion ligand as well as the metal-bound product. **IM7** undergoes ligand exchange with **IMD-1** to release the product and regenerate the active species **IM4** in the form of its mirror invert **IM4′**. **IM4′** converts to **IM5a′**, the mirror invert of **IM5a**, to formally close the catalytic cycle. The free energy profile for the full reaction coordinate beginning with the precatalyst **CAT1** has now been established computationally, with every intermediate and transition state molecularly well-defined and energetically reasonable (Figures 1 and 2). The overall reaction—from **IM5a** through **IM5a′**—is thermodynamically favorable (ΔG = −17.5 kcal/mol), with the largest energy span from **IM6a** to **TS4a** (26.8 kcal/mol). Accordingly, the C−H bond cleavage via **TS4a** is the rate-determining step by computation, which agrees with the experimental observation that C−H bond cleavage might be involved in the rate-determining step. Thus, the calculations demonstrate good experimental−theoretical synergy.

3.3. Ligand Effect on Catalyst Activity. Experimentalists observed that replacement of the ancillary ligand $C_5Me_5^-$ with the unsubstituted $C_5H_5^-$ would significantly deactivate the catalyst, giving only a trace amount of the cycloaddition product (Scheme 1a).[4] This implies that the ancillary Cp ligand exerts an influence on the activity of the catalyst. This kind of Cp ligand effect was first observed in the context of alkene polymerization reactions catalyzed by group 4 (half-)sandwich complexes.[33,34] For example, titanium half-metallocenes show the following order of activity in catalyzing styrene polymerization: $(C_5Me_5)Ti(OMe)_3$ > $(C_5HMe_4)Ti(OMe)_3$ > $(C_5H_5)Ti(OMe)_3$, which indicates the role of electron-donating methyl substituents on the Cp ring in promoting catalysis.[34] The researchers proposed that electron-donating substituents on Cp facilitate alkene insertion into the M−CH_2R bond (the rate-determining step) by weakening the M−CH_2R bond.[33a] A recent report on Sc half-metallocenes disclosed a similar Cp ligand effect; that is, $(C_5Me_4SiMe_3)Sc(CH_2C_6H_4NMe_2\text{-}o)^+$ is more active than $(C_5H_5)Sc(CH_2C_6H_4NMe_2\text{-}o)^+$ in catalyzing the polymerization of 4-benzyloxy-1,6-heptadiene.[35]

To shed light on the ancillary Cp ligand effect on the title reaction, we calculated the complete reaction pathway beginning with the C_5H_5-coordinated **CAT2** (Figure S2), which is analogous to the **CAT1**-catalyzed pathway (Figures 1 and 2) in terms of the elementary steps. However, there are two important differences in the energetics of the reactions, as shown in Figure 3. A higher energy barrier of 30.5 kcal/mol (**IM9** to **TS6**) must be overcome to initiate **CAT2** in comparison with 27.9 kcal/mol (**IM2a** to **TS2a** in Figure 1) that is required to initiate **CAT1**. More importantly, the largest energy span in the **CAT2**-enabled catalytic cycle is from **IM13** to **TS8**, 29.8 kcal/mol, which is significantly greater than 26.8 kcal/mol, the largest energy span in the **CAT1**-enabled catalytic cycle (Figure 2). The difference of 3.0 kcal/mol corresponds to a 1:157 ratio of reaction rates estimated using the Eyring equation;[36] that is, the **CAT2**-catalyzed C−H cycloaddition of **IMD-1** only proceeds at 0.6% of the rate of the **CAT1**-catalyzed reaction under the same conditions. Thus, the calculations clearly account for the experimental observation of the much lower activity of **CAT2** in comparison with **CAT1**. To examine the structural origins of the difference in the activity of **CAT1** and **CAT2**, we focus our attention on the C−H deprotonation transition states **TS4a** and **TS8** (Figures 2−4a), which are the rate-limiting barriers in the **CAT1**- and **CAT2**-catalyzed pathways. The $C_5Me_5^-$ ligand in **TS4a** is more electron-donating than the $C_5H_5^-$ ligand in **TS8**, and because of this inductive effect, the Sc-bound α-carbon in **TS4a** has a higher electron density and stronger basicity than its counterpart in **TS8** and therefore polarizes and deprotonates the imidazole C2−H bond more readily. To further illustrate this point, we compared the contour plots for the Laplacian of the electron density in the Cα−H−C2 plane of **TS4a** and **TS8** (Figure 4b), which were computed using the atoms-in-molecules theory (AIM).[37,38] The electron density around the H atom in **TS4a** is more strongly polarized toward Cα, suggesting a stronger Cα−H bonding interaction in **TS4a**. Thus, the computations illuminate the electronic effect of the ancillary Cp ligands on the activity of **CAT1** and **CAT2**.

The distortion/interaction model[39] can also be invoked to analyze the origins of the difference in the activity of **CAT1** and

https://dx.doi.org/10.1021/acs.joc.0c03054
J. Org. Chem. XXXX, XXX, XXX−XXX

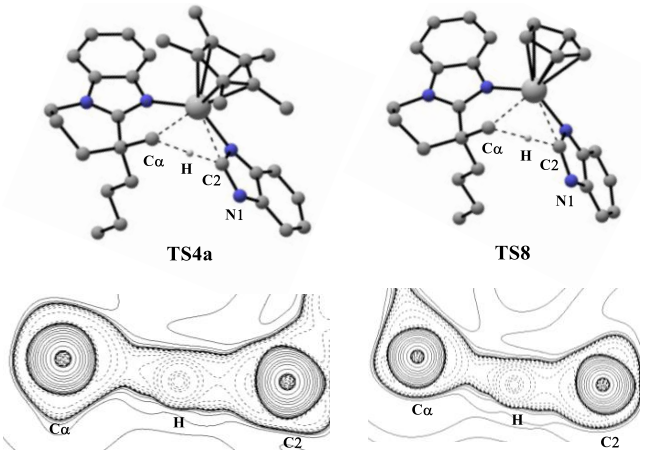

Figure 4. Optimized structures of **TS4a** and **TS8** with all unreactive H atoms and the N1-substituents omitted for clarity (upper part); contour plots of the Laplacian of electron density for **TS4a** and **TS8** in the Cα−H−C2 plane (lower part).

CAT2. The rate-determining **IM6a** → **TS4a** and **IM13** → **TS8** reactions are unimolecular (intramolecular), which can be treated by equating the activation energy and the distortion energy (i.e., $\Delta E^{\ddagger} = \Delta E_{dist}$) because there is no second species to interact with (Figure 5).[40] The calculations show that $\Delta\Delta E^{\ddagger}$ = 2.2 kcal/mol in favor of the **IM6a** → **TS4a** reaction. As indicated by the changes in the distances of the key evolving bonds in the reactants and transition states, the 2.2 kcal/mol difference is mainly caused by the distortion needed for making the Cα−H bond. The Cα−H distance in **IM13** must be contracted 0.1 Å more to attain **TS8** as compared with the **IM6a** → **TS4a** progression. In other words, the Cα−H bond is easier to form as **IM6a** changes to **TS4a**, which might imply the greater electron density on the Cα atom. In any case, the distortion/interaction analysis points to the Cα−H bonding as the origin, which is consistent with the result of the analysis of the contour plots of the Laplacian of electron density (see above).

3.4. Asymmetric Reaction. An asymmetric version of the title reaction was realized by using a chiral catalyst, **CAT3**, which gave a bicyclic imidazole derivative bearing a chiral all-carbon

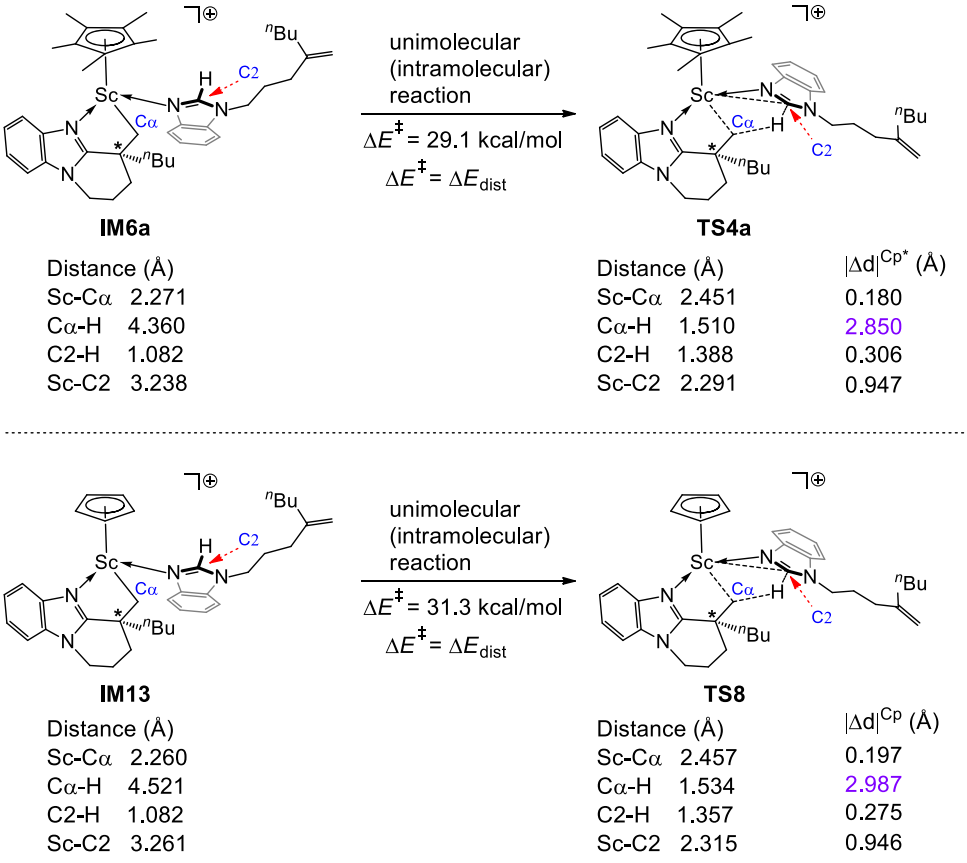

Summary	$\lvert\Delta d\rvert^{Cp} - \lvert\Delta d\rvert^{Cp^*}$ (Å)
Sc-Cα	0.017 ≈ 0.0
Cα-H	0.137 ≈ 0.1
C2-H	-0.031 ≈ 0.0
Sc-C2	-0.001 ≈ 0.0

Figure 5. Distortion/interaction analyses.

https://dx.doi.org/10.1021/acs.joc.0c03054
J. Org. Chem. XXXX, XXX, XXX−XXX

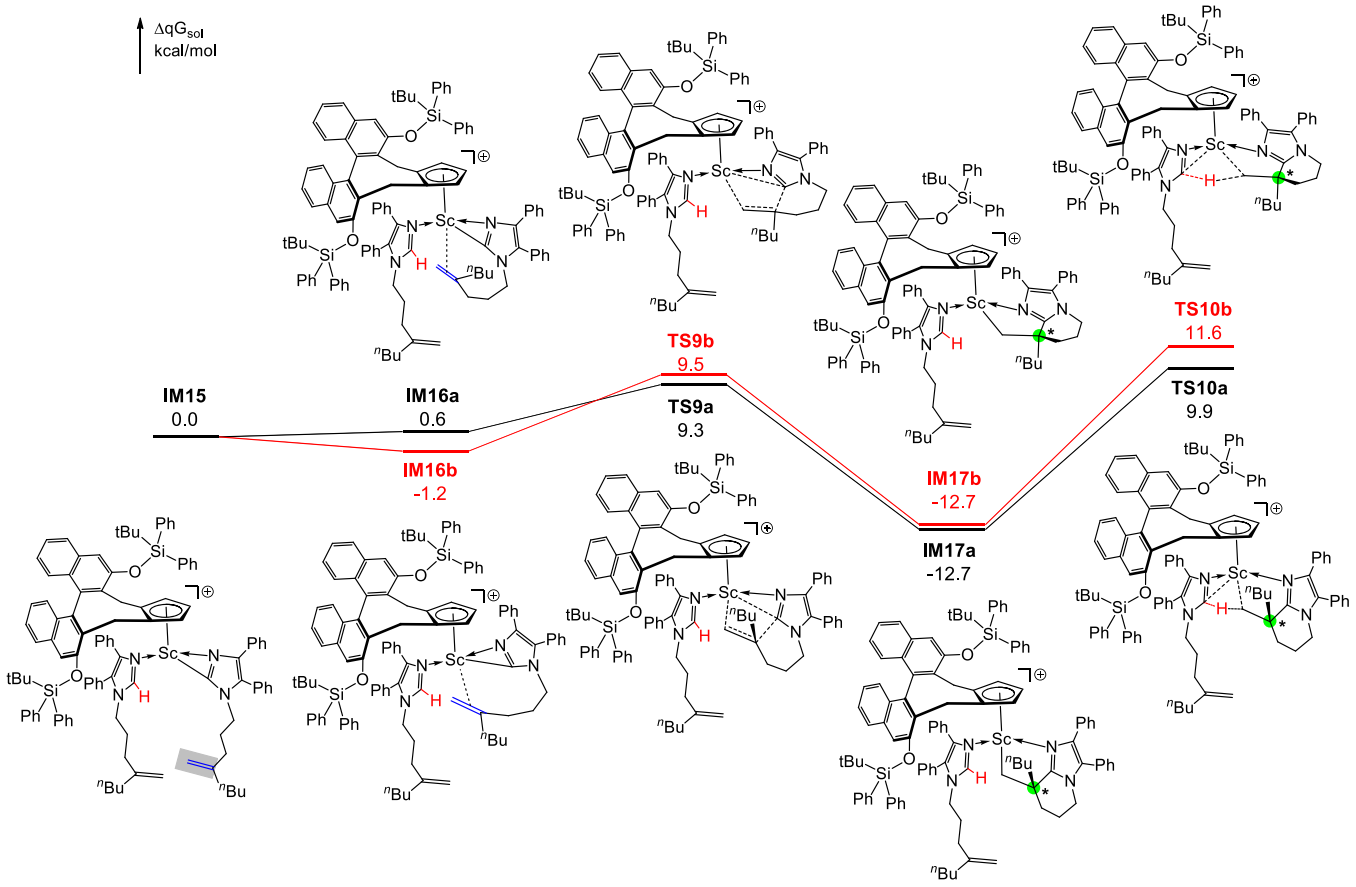

Figure 6. Free energy profile showing the enantioselective steps in the **CAT3**-catalyzed reaction.

quaternary stereocenter with high enantioselectivity (Scheme 1b). Note that the chirality of **CAT3** was imparted by a chiral Cp ligand.[41] With reference to the detailed mechanism established for the reaction (Figures 1 and 2), we seek to unravel the origins of the enantioselectivity.

As shown in Figure 6, we computed the **CAT3**-derived species **IM15**, an analogue to **IM4** (Figure 1). The Sc-bound imidazolyl moiety of **IM15** contains a C═C unit (blue) with two prochiral faces, each of which can bind to the Sc center, thereby forming the diastereomeric π-complexes **IM16a**/**IM16b**. This gives rise to the enantioselective cyclization (C═C insertion) via **TS9a**/**TS9b** and subsequent C2−H bond cleavage via **TS10a**/**TS10b**. The highest barriers **TS10a** and **TS10b**, which lead to the (R)- and (S)-products, respectively, would determine the enantioselectivity. **TS10a** is lower than **TS10b** by 1.7 kcal/mol, suggesting a theoretical enantiomeric ratio of 95:5 in favor of the (R)-product, which agrees qualitatively with the experimental observation (96:4). Comparing the optimized structures of **TS10a** and **TS10b** in Figure 7 reveals the steric bias making **TS10b** a higher energy barrier; that is, **TS10b** contains more steric repulsions occurring between nonbonded H atoms at a distance less than 2.40 Å (two times the van der Waals radius of hydrogen 1.20 Å) than **TS10a**. It is worth noting that experimentalists envisioned diastereomeric complexes similar to **IM16a**/**IM16b** but without the bound imidazole molecule.[4] We have found by computation that such intermediates would be energetically unfavorable (Figure S3).

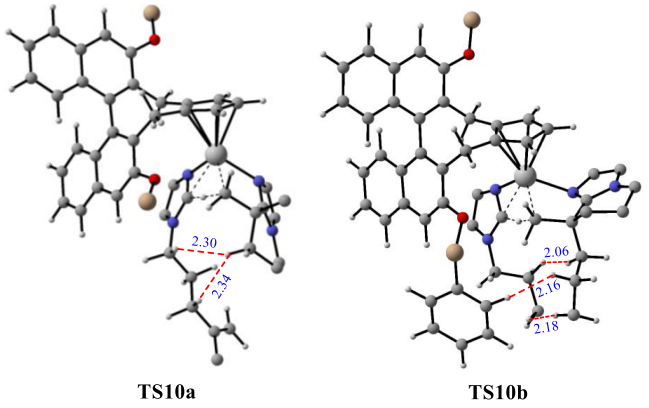

Figure 7. Optimized geometries of **TS10a** and **TS10b** showing steric repulsions between nonbonded H atoms. Peripheral Ph and tBu groups as well as irrelevant H atoms are omitted for clarity.

4. CONCLUSIONS

We have disclosed by DFT computation a detailed mechanism for the newly developed scandium-catalyzed exo-selective C−H cycloaddition of imidazoles to alkenes affording polycyclic imidazole derivatives with all-carbon quaternary stereocenters, as summarized in Scheme 2. The half-sandwich, bis(2-(dimethylamino)benzyl-C,N) Sc complex (**CAT1**) is activated with Ph_3C^+, the resulting cationic complex **IM1** binds the imidazole substrate **IMD-1** strongly, and the adduct **IM2a** enables the Sc-bound α-carbon to cleave the imidazole C2−H bond to form the Sc−imidazolyl complex **IM3**. Ligand exchange with another **IMD-1** molecule converts **IM3** into the catalyst

https://dx.doi.org/10.1021/acs.joc.0c03054
J. Org. Chem. XXXX, XXX, XXX−XXX

Scheme 2. Summary of the Mechanism for Imidazole C−H Cycloaddition to Alkenes

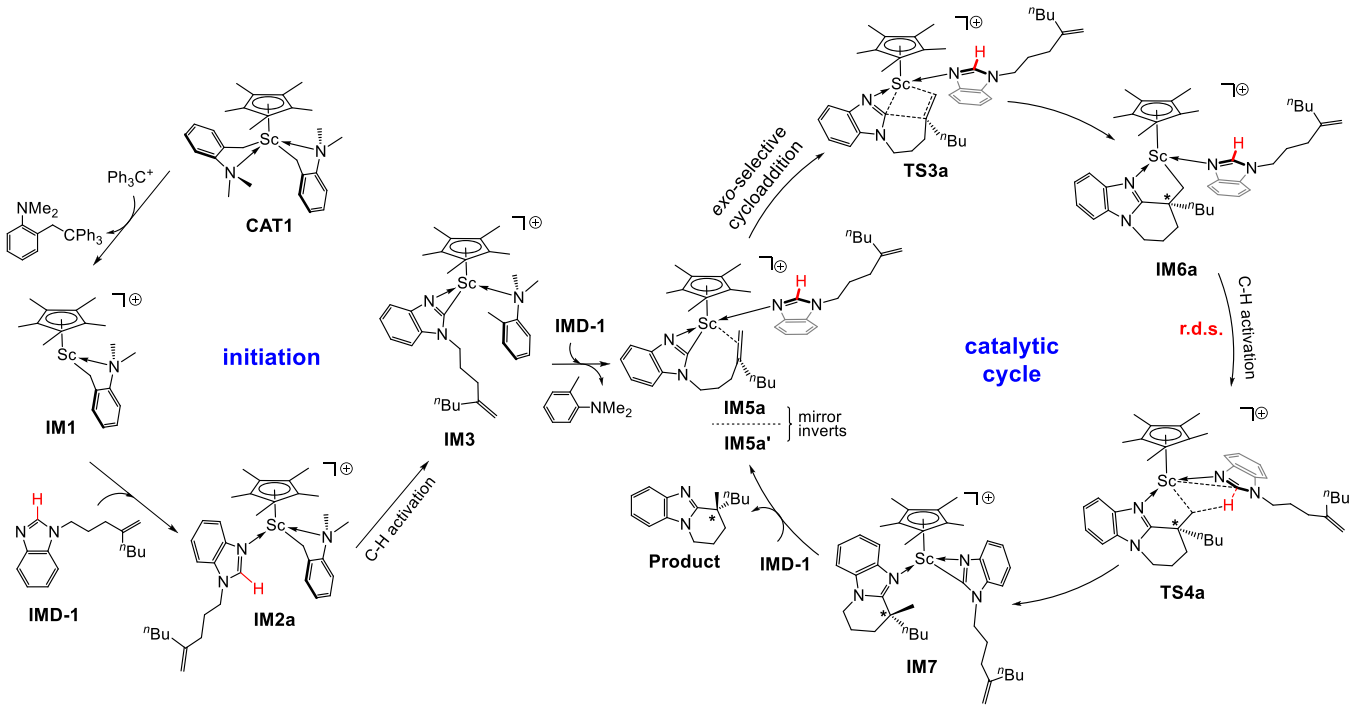

resting state **IM5a**. **IM5a** undergoes intramolecular cyclization (C═C into Sc−imidazolyl insertion) via **TS3a** with exo-selectivity that is governed by ring strain as well as the electronic effect on the C═C bond. This generates a β-all-carbon-substituted quaternary stereocenter in a tricyclic imidazole *N*,*C*-chelator in **IM6a**. The subsequent C−H activation via **TS4a** to form **IM7** serves a dual function: protonating the Sc−C bond to deliver the cycloaddition product and regenerating the active catalyst **IM5a** in the form of its mirror invert **IM5a′**. This rate-determining step defines the largest energy span of the catalytic cycle.

The DFT calculations illuminate the electronic effect of the ancillary Cp ligand on the activity of the catalyst. An electron-rich Cp ligand would increase the electron density and basicity of the Sc-bound α-carbon, thereby facilitating its ability to cleave the imidazole C−H bond. The computations also reveal the steric bias, generated by using a chiral Cp ligand, between the diastereomeric and rate-determining transition states, which induces the enantioselectivity. The insights gained from this theoretical study can be useful for the further development of rare-earth metal-catalyzed C−H functionalization of imidazoles.

■ ASSOCIATED CONTENT

Supporting Information

The Supporting Information is available free of charge at https://pubs.acs.org/doi/10.1021/acs.joc.0c03054.

Additional computational results and energies and Cartesian coordinates of the optimized structures (PDF)

■ AUTHOR INFORMATION

Corresponding Author

Xiaotai Wang − *Hoffmann Institute of Advanced Materials, Postdoctoral Innovation Practice Base, Shenzhen Polytechnic, Nanshan District, Shenzhen 518055, P. R. China; Department of Chemistry, University of Colorado Denver, Denver, Colorado 80217-3364, United States;* orcid.org/0000-0003-3310-3308; Email: xiaotai.wang@ucdenver.edu

Authors

Jiandong Guo − *Hoffmann Institute of Advanced Materials, Postdoctoral Innovation Practice Base, Shenzhen Polytechnic, Nanshan District, Shenzhen 518055, P. R. China; Institute of Theoretical Chemistry, School of Chemistry and Chemical Engineering, Shandong University, Jinan 250100, P. R. China*

Wu Yang − *Hoffmann Institute of Advanced Materials, Postdoctoral Innovation Practice Base, Shenzhen Polytechnic, Nanshan District, Shenzhen 518055, P. R. China; Shenzhen Institutes of Advanced Technology, Chinese Academy of Sciences, Shenzhen 518055, P. R. China*

Dongju Zhang − *Institute of Theoretical Chemistry, School of Chemistry and Chemical Engineering, Shandong University, Jinan 250100, P. R. China;* orcid.org/0000-0002-6117-4958

Shou-Guo Wang − *Shenzhen Institutes of Advanced Technology, Chinese Academy of Sciences, Shenzhen 518055, P. R. China*

Complete contact information is available at: https://pubs.acs.org/10.1021/acs.joc.0c03054

Notes

The authors declare no competing financial interest.

■ ACKNOWLEDGMENTS

We acknowledge support for this work from the Hoffmann Institute of Advanced Materials, Shenzhen Polytechnic, and the University of Colorado Denver.

■ REFERENCES

(1) (a) Ping, Y.; Li, Y.; Zhu, J.; Kong, W. Construction of Quaternary Stereocenters by Palladium-Catalyzed Carbopalladation-Initiated Cascade Reactions. *Angew. Chem., Int. Ed.* **2019**, *58*, 1562−1573.

https://dx.doi.org/10.1021/acs.joc.0c03054
J. Org. Chem. XXXX, XXX, XXX−XXX

(b) Li, Y.; Xu, S. Transition Metal-Catalyzed C-H Functionalization for Construction of Quaternary Carbon Centers. *Chem. - Eur. J.* **2018**, *24*, 16218−16245. (c) Feng, J.; Holmes, M.; Krische, M. J. Acyclic Quaternary Carbon Stereocenters via Enantioselective Transition Metal Catalysis. *Chem. Rev.* **2017**, *117*, 12564−12580. (d) Zeng, X.-P.; Cao, Z.-Y.; Wang, Y.-H.; Zhou, F.; Zhou, J. Catalytic Enantioselective Desymmetrization Reactions to All-Carbon Quaternary Stereocenters. *Chem. Rev.* **2016**, *116*, 7330−7396. (e) Liu, Y.; Han, S.-J.; Liu, W.-B.; Stoltz, B. M. Catalytic Enantioselective Construction of Quaternary Stereocenters: Assembly of Key Building Blocks for the Synthesis of Biologically Active Molecules. *Acc. Chem. Res.* **2015**, *48*, 740−751.

(2) (a) Liang, M. Z.; Meek, S. J. Synthesis of Quaternary Carbon Stereogenic Centers by Diastereoselective Conjugate Addition of Boron-Stabilized Allylic Nucleophiles to Enones. *J. Am. Chem. Soc.* **2020**, *142*, 9925−9931. (b) Estrada, J. G.; Williams, W. L.; Ting, S. I.; Doyle, A. G. Role of Electron-Deficient Olefin Ligands in a Ni-Catalyzed Aziridine Cross-Coupling To Generate Quaternary Carbons. *J. Am. Chem. Soc.* **2020**, *142*, 8928−8937. (c) Wang, Z.-X.; Li, B.-J. Construction of Acyclic Quaternary Carbon Stereocenters by Catalytic Asymmetric Hydroalkynylation of Unactivated Alkenes. *J. Am. Chem. Soc.* **2019**, *141*, 9312−9320. (d) Chen, X.-W.; Zhu, L.; Gui, Y.-Y.; Jing, K.; Jiang, Y.-X.; Bo, Z.-Y.; Lan, Y.; Li, J.; Yu, D.-G. Highly Selective and Catalytic Generation of Acyclic Quaternary Carbon Stereocenters via Functionalization of 1,3-Dienes with CO_2. *J. Am. Chem. Soc.* **2019**, *141*, 18825−18835. (e) Zhang, C.; Santiago, C. B.; Crawford, J. M.; Sigman, M. S. Enantioselective Dehydrogenative Heck Arylations of Trisubstituted Alkenes with Indoles to Construct Quaternary Stereocenters. *J. Am. Chem. Soc.* **2015**, *137*, 15668−15671.

(3) (a) Horatscheck, A.; Andrijevic, A.; Nchinda, A. T.; Le Manach, C.; Paquet, T.; Khonde, L. P.; Dam, J.; Pawar, K.; Taylor, D.; Lawrence, N.; Brunschwig, C.; Gibhard, L.; Njoroge, M.; Reader, J.; van der Watt, M.; Wicht, K.; de Sousa, A. C. C.; Okombo, J.; Maepa, K.; Egan, T. J.; Birkholtz, L.-M.; Basarab, G. S.; Wittlin, S.; Fish, P. V.; Street, L. J.; Duffy, J.; Chibale, K. Identification of 2,4-Disubstituted Imidazopyridines as Hemozoin Formation Inhibitors with Fast-Killing Kinetics and In Vivo Efficacy in the Plasmodium falciparum NSG Mouse Model. *J. Med. Chem.* **2020**, *63*, 13013−13030. (b) Yuan, G.; Qu, X.; Zheng, B.; Neelamegam, R.; Afshar, S.; Iyengar, S.; Pan, C.; Wang, J.; Kang, H. J.; Ondrechen, M. J.; Poutiainen, P.; El Fakhri, G.; Zhang, Z.; Brownell, A.-L. Design, Synthesis, and Characterization of Benzimidazole Derivatives as Positron Emission Tomography Imaging Ligands for Metabotropic Glutamate Receptor 2. *J. Med. Chem.* **2020**, *63*, 12060−12072. (c) Ito, A.; Choi, J.-H.; Takemura, H.; Kotajima, M.; Wu, J.; Tokuyama, S.; Hirai, H.; Asakawa, T.; Ouchi, H.; Inai, M.; Kan, T.; Kawagishi, H. Biosynthesis of the Fairy Chemicals, 2-Azahypoxanthine and Imidazole-4-carboxamide, in the Fairy Ring-Forming Fungus Lepista sordida. *J. Nat. Prod.* **2020**, *83*, 2469−2476. (d) Ali, I.; Lone, M. N.; Aboul-Enein, H. Y. Imidazoles as potential anticancer agents. *MedChemComm* **2017**, *8*, 1742−1773. (e) Denny, R. A.; Flick, A. C.; Coe, J.; Langille, J.; Basak, A.; Liu, S.; Stock, I.; Sahasrabudhe, P.; Bonin, P.; Hay, D. A.; Brennan, P. E.; Pletcher, M.; Jones, L. H.; Chekler, E. L. P. Structure-Based Design of Highly Selective Inhibitors of the CREB Binding Protein Bromodomain. *J. Med. Chem.* **2017**, *60*, 5349−5363. (f) Yadav, G.; Ganguly, S. Structure Activity Relationship (SAR) Study of Benzimidazole Scaffold for Different Biological Activities: A Mini-review. *Eur. J. Med. Chem.* **2015**, *97*, 419−443. (g) Zhang, Z.; Xie, F.; Jia, J.; Zhang, W. Chiral Bicycle Imidazole Nucleophilic Catalysts: Rational Design, Facile Synthesis, and Successful Application in Asymmetric Steglich Rearrangement. *J. Am. Chem. Soc.* **2010**, *132*, 15939−15941.

(4) Lou, S.-J.; Mo, Z.; Nishiura, M.; Hou, Z. Construction of All-Carbon Quaternary Stereocenters by Scandium-Catalyzed Intramolecular C−H Alkylation of Imidazoles with 1,1-Disubstituted Alkenes. *J. Am. Chem. Soc.* **2020**, *142*, 1200−1205.

(5) (a) Diesel, J.; Grosheva, D.; Kodama, S.; Cramer, N. A Bulky Chiral N-Heterocyclic Carbene Nickel Catalyst Enables Enantioselective C-H Functionalizations of Indoles and Pyrroles. *Angew. Chem., Int. Ed.* **2019**, *58*, 11044−11048. (b) Loup, J.; Müller, V.; Ghorai, D.; Ackermann, L. Enantioselective Aluminum-Free Alkene Hydroarylations via C-H Activation by a Chiral Nickel/JoSPOphos Manifold. *Angew. Chem., Int. Ed.* **2019**, *58*, 1749−1753. (c) Tsai, A. S.; Wilson, R. M.; Harada, H.; Bergman, R. G.; Ellman, J. A. Rhodium Catalyzed Enantioselective Cyclization of Substituted Imidazoles via C-H bond Activation. *Chem. Commun.* **2009**, 3910−3912.

(6) (a) Luo, Y.; Ma, Y.; Hou, Z. α-C-H Alkylation of Methyl Sulfides with Alkenes by a Scandium Catalyst. *J. Am. Chem. Soc.* **2018**, *140*, 114−117. (b) Shi, X.; Nishiura, M.; Hou, Z. C-H Polyaddition of Dimethoxyarenes to Unconjugated Dienes by Rare Earth Catalysts. *J. Am. Chem. Soc.* **2016**, *138*, 6147−6150. (c) Nako, A. E.; Oyamada, J.; Nishiura, M.; Hou, Z. Scandium-catalysed intermolecular hydroaminoalkylation of olefins with aliphatic tertiary amines. *Chem. Sci.* **2016**, *7*, 6429−6434. (d) Nagae, H.; Shibata, Y.; Tsurugi, H.; Mashima, K. Aminomethylation Reaction of ortho-Pyridyl C−H Bonds Catalyzed by Group 3 Metal Triamido Complexes. *J. Am. Chem. Soc.* **2015**, *137*, 640−643. (e) Guan, B.-T.; Wang, B.; Nishiura, M.; Hou, Z. Yttrium-Catalyzed Addition of Benzylic C−H Bonds of Alkyl Pyridines to Olefins. *Angew. Chem., Int. Ed.* **2013**, *52*, 4418−4421.

(7) (a) Kundu, A.; Inoue, M.; Nagae, H.; Tsurugi, H.; Mashima, K. Direct ortho-C−H Aminoalkylation of 2-Substituted Pyridine Derivatives Catalyzed by Yttrium Complexes with N,N′ -Diarylethylenediamido Ligands. *J. Am. Chem. Soc.* **2018**, *140*, 7332−7342. (b) Zhan, G.; Teng, H.-L.; Luo, Y.; Lou, S.-J.; Nishiura, M.; Hou, Z. Enantioselective Construction of Silicon-Stereogenic Silanes by Scandium-Catalyzed Intermolecular Alkene Hydrosilylation. *Angew. Chem., Int. Ed.* **2018**, *57*, 12342−12346. (c) Teng, H.-L.; Luo, Y.; Nishiura, M.; Hou, Z. Diastereodivergent Asymmetric Carboamination/ Annulation of Cyclopropenes with Aminoalkenes by Chiral Lanthanum Catalysts. *J. Am. Chem. Soc.* **2017**, *139*, 16506−16509. (d) Luo, Y.; Teng, H.-L.; Nishiura, M.; Hou, Z. Asymmetric Yttrium-Catalyzed C(sp3)-H Addition of 2-Methyl Azaarenes to Cyclopropenes. *Angew. Chem., Int. Ed.* **2017**, *56*, 9207−9210.

(8) Frisch, M. J.; Trucks, G. W.; Schlegel, H. B.; Scuseria, G. E.; Robb, M. A.; Cheeseman, J. R.; Scalmani, G.; Barone, V.; Men-nucci, B.; Petersson, G. A.; Nakatsuji, H.; Caricato, M.; Li, X.; Hratchian, H. P.; Izmaylov, A. F.; Bloino, J.; Zheng, G.; Sonnen-berg, J. L.; Hada, M.; Ehara, M.; Toyota, K.; Fukuda, R.; Hasegawa, J.; Ishida, M.; Nakajima, T.; Honda, Y.; Kitao, O.; Nakai, H.; Vreven, T.; Montgomery, J. A., Jr.; Peralta, J. E.; Ogliaro, F.; Bearpark, M.; Heyd, J. J.; Brothers, E.; Kudin, K. N.; Staroverov, V. N.; Kobayashi, R.; Normand, J.; Raghavachari, K.; Rendell, A.; Burant, J. C.; Iyengar, S. S.; Tomasi, J.; Cossi, M.; Rega, N.; Millam, J. M.; Klene, M.; Knox, J. E.; Cross, J. B.; Bakken, V.; Adamo, C.; Jaramillo, J.; Gomperts, R.; Stratmann, R. E.; Yazyev, O.; Austin, A. J.; Cammi, R.; Pomelli, C.; Ochterski, J. W.; Martin, R. L.; Morokuma, K.; Zakrzewski, V. G.; Voth, G. A.; Salvador, P.; Dannenberg, J. J.; Dapprich, S.; Daniels, A. D.; Farkas, O.; Foresman, J. B.; Ortiz, J. V.; Cioslowski, J.; Fox, D. J. *Gaussian 09*, revision D.01; Gaussian Inc., Wallingford, CT, 2013.

(9) Zhao, Y.; Truhlar, D. G. A new local density functional for main-group thermochemistry, transition metal bonding, thermochemical kinetics, and noncovalent interactions. *J. Chem. Phys.* **2006**, *125*, No. 194101.

(10) Zhao, Y.; Truhlar, D. G. Density Functionals with Broad Applicability in Chemistry. *Acc. Chem. Res.* **2008**, *41*, 157−167.

(11) Kwon, D.-H.; Proctor, M.; Mendoza, S.; Uyeda, C.; Ess, D. H. Catalytic Dinuclear Nickel Spin Crossover Mechanism and Selectivity for Alkyne Cyclotrimerization. *ACS Catal.* **2017**, *7*, 4796−4804.

(12) Qu, S.; Cramer, C. J. Mechanistic Study of Cp^*Co^{III}/Rh^{III}-Catalyzed Directed C−H Functionalization with Diazo Compounds. *J. Org. Chem.* **2017**, *82*, 1195−1204.

(13) Xu, Z.; Xu, J. Z.; Zhang, J.; Zheng, Z. J.; Cao, J.; Cui, Y. M.; Xu, L. W. Mechanistic Insights into Palladium-Catalyzed Silylation of Aryl Iodides with Hydrosilanes through a DFT Study. *Chem. - Asian J.* **2017**, *12*, 1749−1757.

(14) Bai, H.; Xu, H.; Zhang, H.; Guo, Y.; Shan, J.; Wei, D.; Zhu, Y.; Zhang, S.; Zhang, W. Theoretical investigations of the Ir-catalyzed direct borylation of B(3,6)−H of *o*-carborane: the actual catalyst,

https://dx.doi.org/10.1021/acs.joc.0c03054
J. Org. Chem. XXXX, XXX, XXX−XXX

mechanism, and origin of regioselectivity. *Catal. Sci. Technol.* **2018**, *8*, 5165−5177.
(15) Mondal, T.; De, S.; Dutta, S.; Koley, D. Mechanistic Exploration of the Transmetalation and Reductive Elimination Events Involving $Pd^{(IV)}$ -Abnormal NHC Complexes in Suzuki-Miyaura Coupling Reactions: A DFT Study. *Chemistry* **2018**, *24*, 6155−6168.
(16) Li, B.-w.; Wang, M.-y.; Fang, S.; Liu, J.-y. DFT Study on the Mechanism of Palladium(0)-Catalyzed Reaction of Aryl Iodides, Norbornene, and Di-*tert*-butyldiaziridinone. *Organometallics* **2019**, *38*, 2189−2198.
(17) Besalú-Sala, P.; Magallon, C.; Costas, M.; Company, A.; Luis, J. M. Mechanistic Insights into the *ortho*-Defluorination-Hydroxylation of 2-Halophenolates Promoted by a Bis(α-oxo)dicopper(III) Complex. *Inorg. Chem.* **2020**, *59*, 17018−17027.
(18) Gorantla, K. R.; Mallik, B. S. Computational mechanistic study on molecular catalysis of water oxidation by cyclam ligand-based iron complex. *Theor. Chem. Acc.* **2020**, *139*, No. 161.
(19) Orsino, A. F.; Moret, M.-E. Nickel-Catalyzed Alkyne Cyclotrimerization Assisted by a Hemilabile Acceptor Ligand: A Computational Study. *Organometallics* **2020**, *39*, 1998−2010.
(20) Huang, C.; Huang, L.; Li, G.; Xie, Y.; King, R. B.; Schaefer, H. F. Fluorine Migration from Carbon to Iron and Fluorine−Iron Dative Bonds in Octafluorocyclohexadiene Iron Carbonyl Chemistry. *Organometallics* **2021**, *40*, 397−407.
(21) Li, J.; Yang, Y.; Di, H.; Wang, J. Cascade Hydrogenation-Cyclization of Levulinic Acid into γ-Valerolactone Catalyzed by Half-Sandwich Iridium Complexes: A Mechanistic Insight from Density Functional Theory. *J. Org. Chem.* **2021**, *86*, 674−682.
(22) (a) Grimme, S.; Antony, J.; Ehrlich, S.; Krieg, H. A consistent and accurate ab initio parametrization of density functional dispersion correction (DFT-D) for the 94 elements H−Pu. *J. Chem. Phys.* **2010**, *132*, 154104−154119. (b) Goerigk, L.; Mehta, N. A Trip to the Density Functional Theory Zoo: Warnings and Recommendations for the User. *Aust. J. Chem.* **2019**, *72*, 563−573.
(23) Marenich, A. V.; Cramer, C. J.; Truhlar, D. G. Universal Solvation Model Based on Solute Electron Density and on a Continuum Model of the Solvent Defined by the Bulk Dielectric Constant and Atomic Surface Tensions. *J. Phys. Chem. B* **2009**, *113*, 6378−6396.
(24) Ribeiro, R. F.; Marenich, A. V.; Cramer, C. J.; Truhlar, D. G. Use of Solution-Phase Vibrational Rrequencies in Continuum Models for the Free Energy of Solvation. *J. Phys. Chem. B* **2011**, *115*, 14556−14562.
(25) Lu, T.; Chen, Q. Shermo: A general code for calculating molecular thermodynamic properties *ChemRxiv* 2020, DOI: 10.26434/chemrxiv.12278801.
(26) Riplinger, C.; Pinski, P.; Becker, U.; Valeev, E. F.; Neese, F. Sparse maps—A systematic infrastructure for reduced-scaling electronic structure methods. II. Linear scaling domain based pair natural orbital coupled cluster theory. *J. Chem. Phys.* **2016**, *144*, No. 024109.
(27) Legault, C. Y. *CYLView, 1.0b*; Université de Sherbrooke: Quebec, Montreal, Canada, 2009, http://www.cylview.org.
(28) Lu, T.; Chen, F. Multiwfn: A Multifunctional Wavefunction Analyzer. *J. Comput. Chem.* **2012**, *33*, 580−592.
(29) Cao, X.; Rong, C.; Zhong, A.; Lu, T.; Liu, S. Molecular acidity: An accurate description with information-theoretic approach in density functional reactivity theory. *J. Comput. Chem.* **2018**, *39*, 117−129.
(30) We also considered the substitution of the arylamine byproduct from the CAT1 → IM1 step, whichwould be much less exergonic (ΔG = −0.5 kcal/mol) and could be ruled out.
(31) One prochiral face of the alkene is arbitrarily chosen to bind to scandium.
(32) (a) Kozuch, S.; Shaik, S. How to Conceptualize Catalytic Cycles? The Energetic Span Model. *Acc. Chem. Res.* **2011**, *44*, 101−110. (b) Kozuch, S.; Shaik, S. A combined kinetic−quantum mechanical model for assessment of catalytic cycles: Application to cross-coupling and Heck reactions. *J. Am. Chem. Soc.* **2006**, *128*, 3355−3365.
(33) (a) Möhring, P. C.; Coville, N. J. Quantification of the influence of steric and electronic parameters on the ethylene polymerisation activity of $(CpR)_2ZrCl_2$/ethylaluminoxane Ziegler−Natta catalysts. *J. Mol. Catal.* **1992**, *77*, 41−50. (b) Möhring, P. C.; Coville, N. J. Homogeneous group 4 metallocene ziegler-natta catalysts: The influence of cyclopentadienyl-ring substituents. *J. Organomet. Chem.* **1994**, *479*, 1−29.
(34) Tomotsu, N.; Ishihara, N.; Newman, T. H.; Malanga, M. T. Syndiospecific polymerization of styrene. *J. Mol. Catal. A: Chem.* **1998**, *128*, 167−190.
(35) Wang, H.; Zhao, Y.; Nishiura, M.; Yang, Y.; Luo, G.; Luo, Y.; Hou, Z. Scandium-Catalyzed Regio- and Stereoselective Cyclopolymerization of Functionalized α,ω-Dienes and Copolymerization with Ethylene. *J. Am. Chem. Soc.* **2019**, *141*, 12624−12633.
(36) Atkins, P.; de Paula, J.; Keeler, J. *Atkins' Physical Chemistry*, 11th ed.; Oxford University Press, 2018.
(37) (a) Bader, R. F. W. *Atoms in Molecules: A Quantum Theory*; Oxford University Press: New York, 1994. (b) Bader, R. F. W. A quantum theory of molecular structure and its applications. *Chem. Rev.* **1991**, *91*, 893−928.
(38) (a) Liu, F.; Zhu, L.; Zhang, T.; Zhong, K.; Xiong, Q.; Shen, B.; Liu, S.; Lan, Y.; Bai, R. Nucleophilicity versus Brønsted Basicity Controlled Chemoselectivity: Mechanistic Insight into Silver- or Scandium-Catalyzed Diazo Functionalization. *ACS Catal.* **2020**, *10*, 1256−1263. (b) Schwarzer, M. C.; Fujioka, A.; Ishii, T.; Ohmiya, H.; Mori, S.; Sawamura, M. Enantiocontrol by assembled attractive interactions in copper-catalyzed asymmetric direct alkynylation of α-ketoesters with terminal alkynes: OH···O/sp3-CH···O two-point hydrogen bonding combined with dispersive attractions. *Chem. Sci.* **2018**, *9*, 3484−3493. (c) Lin, Z.; Hall, M. B. Electron density analysis of the transition states of substitution reactions of 17- and 18-electron hexacarbonyl complexes. *J. Am. Chem. Soc.* **1992**, *114*, 6574−6575.
(39) Bickelhaupt, F. M. Understanding Reactivity with Kohn-Sham MO Theory: The E2-SN2 Mechanistic Spectrum and other Concepts. *J. Comput. Chem.* **1999**, *20*, 114−128.
(40) Bickelhaupt, F. M.; Houk, K. N. Analyzing Reaction Rates with the Distortion/Interaction-Activation Strain Model. *Angew. Chem., Int. Ed.* **2017**, *56*, 10070−10086.
(41) Opposite configurations of the chiral Cp ligand were given in the main text and supporting information of ref. 4. The authors of ref. 4 clarified the confusion in private communications with us: the configuration shown in the supporting information was correct. We used the correct configuration for calculations.

https://dx.doi.org/10.1021/acs.joc.0c03054
J. Org. Chem. XXXX, XXX, XXX−XXX